JACS
JOURNAL OF THE AMERICAN CHEMICAL SOCIETY

ARTICLE

pubs.acs.org/JACS

Coupled Commensurate Cation and Charge Modulation in the Tunneled Structure, $Na_{0.40(2)}MnO_2$

Izabela Kruk,[†,‡] Pawel Zajdel,[§] Wouter van Beek,[∥,⊥] Ioanna Bakaimi,[#,¶] Alexandros Lappas,[#] Chris Stock,[†,▽] and Mark A. Green*[,†,○]

[†]NIST Center for Neutron Research, National Institute of Standards and Technology, Gaithersburg, Maryland 20899, United States

[‡]Christopher Ingold Laboratory, University College London, 20 Gordon Street, London WC1H 0AJ, United Kingdom

[§]Department of Physics of Crystals, University of Silesia Uniwersytecka 4, 40-007 Katowice, Poland

[∥]European Synchrotron Radiation Facility, 6 rue Jules Horowitz, BP 220, 38043 Grenoble Cedex, France

[⊥]Dipartamento di Scienze e Technologie Avanzate, Universita del Piemonte Orientale and NanoSistemi IC, Via Bellini 25/G, I-15100 Alessandria, Italy

[#]Institute of Electronic Structure and Laser, FORTH, 711 10 Heraklion, Greece

[¶]Department of Physics, University of Crete, GR-71003 Heraklion, Greece

[▽]Indiana University, 2401 Milo B. Sampson Lane, Bloomington, Indiana 47408, United States

[○]Department of Materials Science and Engineering, University of Maryland, College Park, Maryland 20742-2115, United States

Supporting Information

ABSTRACT: $Na_{0.40(2)}MnO_2$ belongs to a family of mixed Mn^{3+} and Mn^{4+} porous oxides that contains both octahedral and square pyramidal Mn−O units. Neutron and synchrotron radiation studies identify the presence of both sodium ordering ($T_{Na} \approx 310$ K) and Mn charge and orbital ordering. Below T_{Na}, the centrosymmetric *Pbam* structure adopts an (a b $4c$) supercell of *Pnnm* symmetry that accommodates a coupled commensurate modulation down the c-axis channels of both Na position and occupancy with Mn valence.

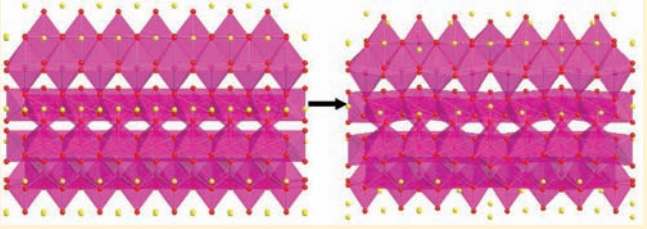

INTRODUCTION

Manganese oxides have proved to be a versatile family of compounds in the study of strongly correlated electron systems, and, in particular, the investigation of the interplay between charge, orbital, and structural degrees of freedom.[1,2] Some mixed Mn^{3+}/Mn^{4+} perovskites show the colossal magnetoresistance effect as a result of Zener double exchange,[3] whereas many systems possess localized charge leading to the Jahn−Teller active Mn^{3+} undergoing axial elongation and ferro-orbital ordering of the $d_{3r^2-z^2}$ orbitals.[4] This phenomenon has been observed in many structure types, such as the perovskites, $LaMnO_3$, where destruction of the Jahn−Teller distortion and orbital ordering occurs at 750 K.[5] Orbital ordering occurs as high as 750−770 K for $BiMnO_3$,[6] where the polarizability of the Bi 6s lone pair plays an important role.[7] Recently, layered manganates have been studied, such as α-$NaMnO_2$[8,9] and Ag_2MnO_2,[10] that show similar orbital ordering, albeit at much lower temperatures, along with low dimensional magnetic order. These layered compounds are precursors to manganese oxides with tunnel structures, whose electronic properties have been much less studied, but have potentially unique properties as a result of the complex arrangement of corner- and edge-shared Mn−O units.[11] $Na_{0.44}MnO_2$ was first identified in the Na_xMnO_2 phase diagram by Parant et al. as the thermodynamical stable high temperature phase for $x \ll 0.5$.[12] This structure has subsequently received attention as a potential material for use in lithium-ion batteries, when the Na ions in the pores are replaced with Li.[13−15] Recently, a single crystal X-ray study revealed that Na positioning is more complex than first reported by Parant et al., although the quadrupled supercell was not observed.[16] A coupling between the charge on the manganese sites and cation ordering has previously been seen in the tunneled structure, $CaMn_3O_6$,[17] which is isostructural with $CaFe_2O_4$,[18] but possesses Ca vacancies in addition to the charge and orbital ordering. The variable occupancy of cation sites within the tunnels often leads to incommensurate properties, such as in $SrMn_3O_6$.[19] Here, we show that the tunnel structure of $Na_{0.40(2)}MnO_2$ possesses an unusual temperature dependence for both the cation and the orbital ordering transitions, which couple to form a complex modulated structure at low temperature best described in the *Pnnm* space group with a cell that is (a b $4c$) with respect to unit cell at 500 K. $Na_{0.40(2)}MnO_2$ is part of a large family of complex porous manganese oxides,[20,21] whose detailed structures may hold interesting new relationships on the interplay between structure and electronic ordering.

Received: October 28, 2010
Published: July 29, 2011

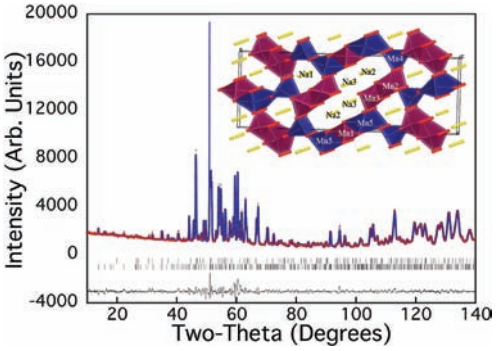

Figure 1. Observed, calculated, and difference spectra of $Na_{0.40(2)}MnO_2$ at 500 K as obtained from Rietveld analysis of powder neutron diffraction data. Inset: Structure of $Na_{0.40(2)}MnO_2$ at 500 K as determined from powder neutron diffraction.

Table 1. Atomic Positions of $Na_{0.40(2)}MnO_2$ at 500 K As Determined from Rietveld Analysis of Powder Neutron Diffraction Data[a]

atom	*x*	*y*	*z*	occupancy
Mn1	0.0 (−)	0.5 (−)	0.0 (−)	1 (−)
Mn2	0.3754 (13)	0.3043 (4)	0.5 (−)	1 (−)
Mn3	0.0198 (11)	0.1118 (4)	0.0 (−)	1 (−)
Mn4	0.0413 (11)	0.3082 (4)	0.0 (−)	1 (−)
Mn5	0.3614 (12)	0.0873 (4)	0.5 (−)	1 (−)
O1	0.3612 (8)	0.0000 (3)	0.5 (−)	1 (−)
O2	0.2193 (9)	0.0958 (3)	0.5 (−)	1 (−)
O3	0.0402 (9)	0.1582 (3)	0.0 (−)	1 (−)
O4	0.4304 (8)	0.1653 (4)	0.5 (−)	1 (−)
O5	0.1717 (8)	0.2842 (3)	0.5 (−)	1 (−)
O6	0.4239 (8)	0.2657 (3)	0.0 (−)	1 (−)
O7	0.3238 (8)	0.3546 (3)	0.0 (−)	1 (−)
O8	0.4973 (8)	0.0733 (3)	0.0 (−)	1 (−)
O9	0.4820 (8)	0.4319 (3)	0.5 (−)	1 (−)
Na1	0.219 (3)	0.2065 (8)	0.0 (−)	0.82 (3)
Na2	0.237 (4)	0.424 (1)	0.5 (−)	0.39 (3)
Na3	0.128 (3)	0.0025 (9)	0.0 (−)	0.61 (3)

[a] Lattice parameters were a = 9.1063(3) Å, b = 26.4235(9) Å, and c = 2.82700(9) Å. R-factor = 6.16%. Space group, *Pbam*.

EXPERIMENTAL DETAILS

Powder samples of nominal composition, $Na_{0.44}MnO_2$, were synthesized by mixing commercial Na_2CO_3 with Mn_2O_3 and heating at 800 °C for 24 h in air, followed by a regrinding and second heating at the same temperature for 9 h. The reaction of the starting materials that were performed in an Na:Mn ratio of 0.44:1 always leads to a few percent by weight of an Mn_2O_3 impurity, presumably as a result of Na loss during the sintering process. No improvement was found on performing the synthesis at different temperatures or heating times. Performing the reaction at lower temperatures led to unreactive starting material and/or poor crystallinity, whereas higher temperatures produced greater amounts of the Mn_2O_3 impurity. Making the reaction significantly more Na rich made only modest improvements to the phase purity, and the Mn_2O_3 impurity remained. A more effective solution to eradicate the Mn_2O_3 impurity was found by adding additional amounts of Na in a two-step process. First, a 3% molar excess of Na_2CO_3 was added before the initial 800 °C heating, followed by a second addition of 2% molar excess of faster decomposing NaOH for the second 9 h heating procedure. This eliminated the presence of the Mn−O phase, but left small unreacted quantities of Na_2CO_3 in the sample. Reduction of the excess amount of Na in either step led to the coexistance of the carbonate and unreacted Mn_2O_3 impurities, but as future magnetic studies would be unaffected by the Na_2CO_3 impurity, in contrast to the magnetic Mn_2O_3 impurity, the structural work was performed with samples containing a slight excess of Na_2CO_3. The material was handled and stored under an inert gas to avoid water absorption within the pores. The actual composition was determined to be $Na_{0.40(2)}MnO_2$ from a combination of prompt gamma neutron activation analysis and neutron diffraction experiments. Powder neutron diffraction data were collected on the BT1 diffractometer at the NIST Center for Neutron Research, National Institute of Standards and Technology, Gaithersburg, MD, using the Ge (311) monochromator at λ = 2.0878 Å. Synchrotron radiation diffraction measurements were performed on the Swiss-Norweigian beamline (λ = 0.723227 Å, T = 100−500 K, 300−1000 K) and the ID31 beamline (λ = 0.399861 Å, T = 5 K) at the European Synchrotron Radiation Facility, Grenoble, France. Rietveld refinement was performed using the Fullprof suite of programs.[22]

RESULTS AND DISCUSSION

High Temperature Structure. Synchrotron measurements, discussed later, showed the presence of a transition around ambient temperature, so the first structure was solved from powder neutron diffraction data taken at T = 500 K. The results of the refinements of $Na_{0.40(2)}MnO_2$ are shown in Figure 1, which is isostructural with $Na_4Mn_4Ti_5O_{18}$,[23] and possesses the centrosymmetric *Pbam* space group. Table 1 lists the atomic coordinates determined from this model. The lattice parameters at 500 K were a = 9.1063(3) Å, b = 26.4235(9) Å, and c = 2.8270(9) Å. At this temperature, the structure contains five crystallographically independent Mn sites, four of which are octahedral, labeled Mn1, Mn2, Mn3, and Mn5, while the remaining one has square pyramidal coordination and is labeled Mn4. Mn5−Mn1−Mn5 form a section of three edge-shared octahedra that could be described as a (3 × 1 × ∞) Mn−O block. Similarly, Mn3−Mn2 octahedra form a pair of edge-shared octahedral that could be written as a (2 × 1 × ∞) Mn−O block. Both of these structural units can be thought of as sections of the two-dimensional manganate, α-$NaMnO_2$,[12] which possesses edge-shared (∞ × ∞ × 1) layers. These blocks in $Na_{0.40(2)}MnO_2$ are corner-shared to each other, as well as being bridged by the Mn4 square pyramid that only possesses corner-shared bonding. The 2-fold rotation axis down the c axis generates an additional 6 Mn−O units at 180° to form an "S" shaped channel that contains 10 MnO_6 and 2 MnO_5 units in total. These "S" shaped channels are joined together by a diagonal row of a smaller secondary channel that is made up of four octahedral and two square pyramid Mn−O units. The Na ions occupy both channels. The first within the small spherical channel, labeled Na1 in Figure 1 and Table 1, is 82(3)% occupied and located on the unit cell edge at z = 0. The "S" shaped channel contains two positions; the first, labeled Na2 in Figure 1 and Table 1, is 39(3)% occupied and is located furthest from the middle of the channel, but in the center of the c-axis at z = 0.5. A second position that is 61(3) % occupied, labeled Na3 in Figure 1 and Table 1, is close to the middle of the channel and like Na1 sits on the unit cell edge at z = 0. Both Na2 and Na3 have symmetrically equivalent second sites within the "S" shape channels that are generated by the 2-fold rotation axis. The tendency for the Na ions to prefer

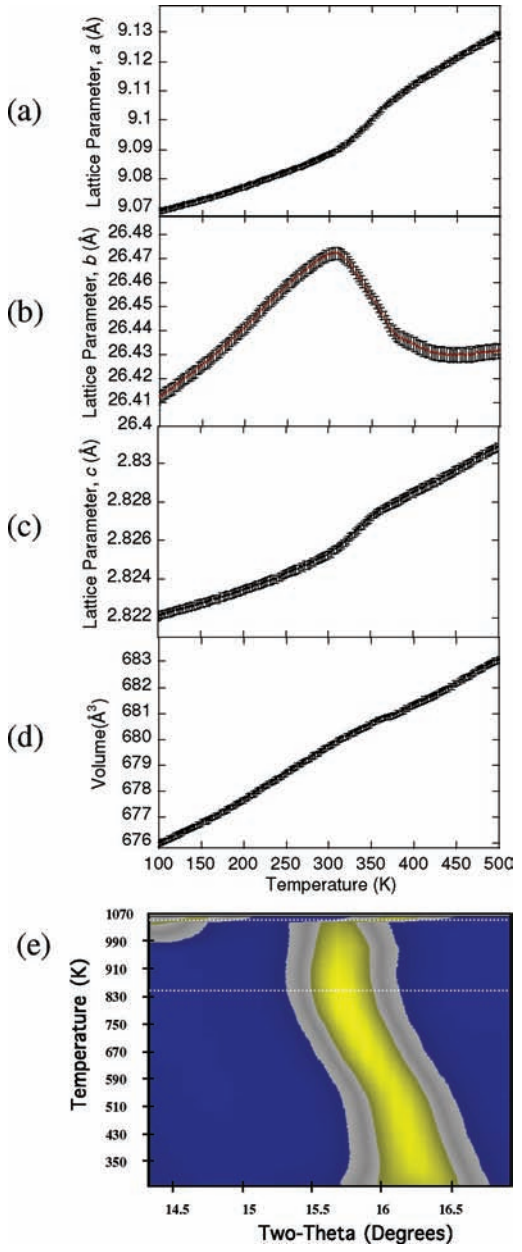

Figure 2. (a–d) Lattice parameters *a*, *b*, and *c* and volume as a function of temperature from 100 to 500 K, showing an anomaly around 310 K. These changes are accompanied by addition superlattice reflections and are associated with the ordering of Na within the channels. (e) Contour map of a section of the powder X-ray diffraction pattern showing an inflection below 840 K, resulting in a further transition.

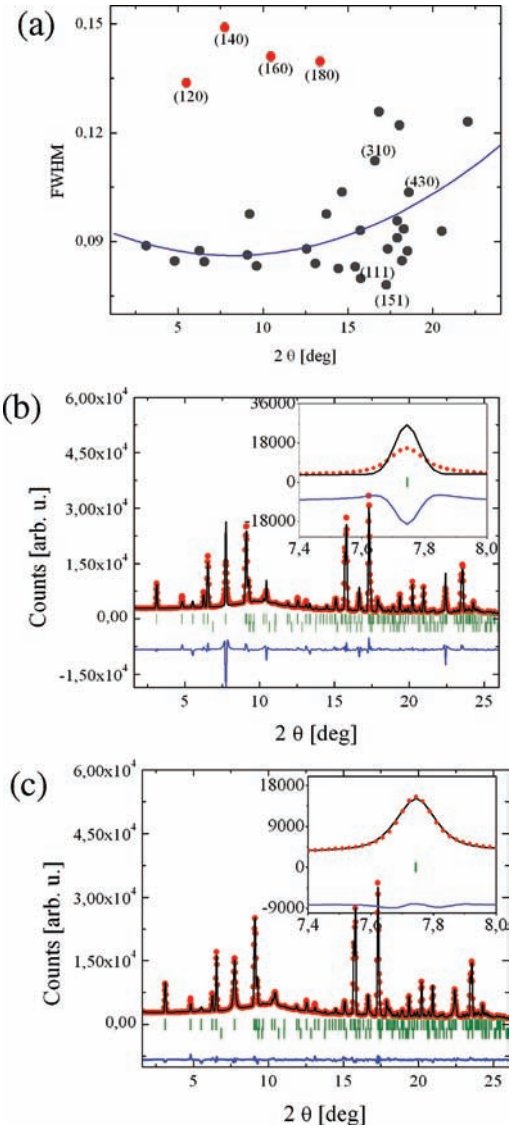

Figure 3. Initial Rietveld refinement was hindered by anisotropic broadening of groups of reflections as shown by the deviation from the resolution function of a number of reflections in (a). The blue line represents an average fwhm. A multiple anisotropic broadening model was found to appropriately account for these stacking faults and gave a good fit (shown in (c)) as compared to the fit without isotropic broadening of reflections, which is shown in (b).

central locations within the "S" shaped channel is consistent with the dynamical motion of the Na ions at these elevated temperatures. Bond distance analysis, summarized in the Supporting Information, shows that the Mn1, Mn2, and Mn3 octahedra possess regular Mn−O bond distances that are typical for Mn^{4+} ions. For example, calculation of the bond distance variance, a measure of the extent that each Mn−O deviates from an average, gives values of 0.01, 0.04, and 0.04 for Mn1, Mn2, and Mn3, respectively, suggesting the absence of a Jahn−Teller distortion. In contrast, the square pyramid Mn4 and octahedral Mn5 show bonding more consistent with the Jahn−Teller active Mn^{3+} ion ordering of the e_g electron in the $d_{3r^2-z^2}$ orbital. In these configurations, Mn4 and Mn5 have contrasting bond lengths with some of their Mn−O bonds above 2.1 Å, and their bond length variance is now 0.076 and 0.132, respectively. Mn1 has a multiplicity of 2, whereas all other Mn sites have a multiplicity of 4. Therefore, Mn1, Mn2, and Mn3 that are more Mn^{4+} in character make up 60% of the sites, whereas Mn^{3+} ions, Mn4, and Mn5 amount to 40%, which is consistent with the amount of Na doped into the channels. The formula can be best written as $Na_{0.4}{}^{+}Mn_{0.4}{}^{3+}Mn_{0.6}{}^{4+}O_2$. Of course, charge ordered systems rarely show complete valence separation, but this does provide a description that helps in the understanding of the relative charges across the Mn sites.

Temperature Dependence. To explore the temperature dependence of the structure, a series of synchrotron experiments

were performed from 100 to 500 K and from 300 to 1000 K on the Swiss-Norwegian beamline. Figure 2a−d shows the lattice parameters and volume changes from 100 to 500 K. A clear anomaly occurs at around 310 K, particularly along the *b*-axis. This was concomitant with the appearance of superlattice reflections that were assumed to be associated with ordering of the Na ions, as Na orders at similar temperatures in other structures. Figure 2e shows a point of inflection below around 840 K, a temperature that melting of charge and orbital ordering occurs in related systems. A further series of neutron experiments were performed to confirm the origin of this broad transition from 600 to 850 K. However, above ~700 K additional shoulders grew next to some but not all of the major reflections. In addition, attempts to perform Rietveld analysis showed strong evidence of Na loss even at these temperatures. These findings suggest that a first-order transition to a different phase, and most likely of different symmetry, is occurring but is incomplete and developing as intergrowths. This, coupled with the fact that some Na loss is already occurring, makes it impossible to derive any conclusive information from an averaging technique like diffraction. However, given the temperature that the melting of the charge and orbital ordering occurs in other structure types, one can speculate that this transition is likely to be a combination of Na loss and melting of Mn^{3+}/Mn^{4+} order. Further information may be gained from the use of a local probe, such as electron microscopy.

During the Rietveld analysis of the data between 80 and 500 K, one key difference with the synchrotron data, as compared to the neutron diffraction data, was the presence of very significant anisotropic broadening. Figure 3a shows a plot of the full width at half-maximum as a function of diffraction angle for $Na_{0.40(2)}MnO_2$ taken at 350 K and above the Na ordering temperature. An average fit to these widths is given as a guide to the eye. A complex relationship was evident such that a satisfactory fit was only possible with the inclusion of a number of custom anisotropic broadening terms, particularly to the $(h\,2k\,0)$ reflections. A model where a number of reflections groups met the general condition $n_1h + n_2k + n_3l = n_4n + n_5$, where n_{1-5} are user defined parameters and n is an integer, was implemented. Figure 3b and c shows the refinements with and without the anisotropic broadening terms, demonstrating the level of improvement achieved with the use of these additional parameters. The anisotropic broadening terms were used further in the high-resolution synchrotron measurements described in the following section.

The limited *Q*-range for these rapid collection scans on the Swiss-Norwegian beamline prevented a full refinement of the atomic positions or indexing of the superlattice reflections, so the low temperature sodium ordered structure was explored with further synchrotron measurements on the ID31 beamline. Temperature-dependent measurements of the superlattice reflections from 80 to 500 K (shown in the Supporting Information) showed very little change as a function of temperature until T_{Na}, where there is an abrupt transition to a state with disordered Na ions and absence of superlattice reflections. This suggests that the structure locks into a very specific configuration below T_{Na}, with little evolution as the material is cooled to base. We will, therefore, concentrate on the lowest temperature structure at 5 K.

Low Temperature Structure. *Symmetry and Nomenclature.* The high-resolution synchrotron data from ID31 at 5 K showed numerous superlattice reflections that could be indexed on a $(a\,b\,4c)$ cell using the Supercell program within Fullprof.[22] The maximum subgroups of the original *Pbam* cell, as obtained using

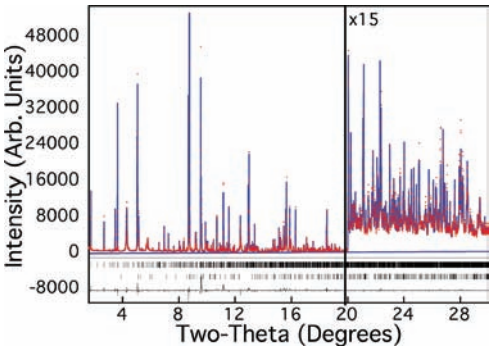

Figure 4. Observed, calculated, and difference spectra of $Na_{0.40(2)}MnO_2$ at 5 K as obtained from Rietveld analysis of synchrotron X-ray diffraction data.

MAXSUB program,[24] showed two possibilities to derive a four times cell, both in a two-stage process. First, doubling of *c* can be achieved in the following groups: *Pbam*, *Pbam* with translation, *Pnnm* and *Pnnm* with translation. However, the second doubling of the *c* axis is only feasible in the *Pbam* space group, which leads to *Pnnm* or *Pbam* as possible space groups for the $(a\,b\,4c)$ cell. A summary of the possible symmetry transformations is given in the Supporting Information, along with some examples of how well the superlattice reflections were described in this quadrupled cell. Both configurations of the $(a\,b\,4c)$ cell, *Pbam* (space group number 55) and *Pnnm* (space group number 58), gave markedly improved fits to the refinement. However, the presence of the (013) reflection at around 6.15° and the (073) reflection at 8.59° showed that the $(0\,k\,l)$: $k + l$ symmetry condition for the *Pnnm* space group is preferred over the $(0\,k\,l)$: k symmetry condition for the *Pbam* space group. Therefore, the refinement was performed in the *Pnnm* space group.

The observed, calculated, and difference spectra obtained using this model are shown in Figure 4, and the atomic coordinates at 5 K are listed in Table 2. The structure now has 43 inequivalent atoms in the unit cell. In the high temperature, structure atoms can be divided into two categories: those at the cell edge with coordinate $(x\,y\,0)$ and those in the cell center with coordinates $(x\,y\,0.5)$. On transforming to the supercell with a quadruple *c* axis, those at $(x\,y\,0)$ split into three new positions with coordinates $(x\,y\,0)$, $(x\,y\,\sim0.25)$, and $(x\,y\,0.5)$: two on special positions and one on a general position. The atoms at $(x\,y\,0.5)$ in the high temperature structure generate two new positions at low temperature with coordinates $(x\,y\,\sim0.125)$ and $(x\,y\,\sim0.625)$, both of which are general positions. For example, the 5 Mn chains in the high temperature structure shown in Figure 1 split into 13 independent Mn positions; Mn1, Mn3, and Mn4 that have high temperature coordinates of $(x\,y\,0)$ each produce three inequivalent Mn ions at low temperature, whereas Mn2 and Mn5 that were positioned with coordinates of $(x\,y\,0.5)$ at high temperature produce just two new Mn ions. Similarly, Na1 and Na3 generate three new Na positions, whereas Na2 generates just two, making a total of eight Na positions in the low temperature structure. To simplify the nomenclature, we follow the scheme that Mn1 (high temperature) produces Mn11, Mn12, and Mn13 at low temperature and Na2 (high temperature) produces Na21 and Na22 at low temperature and so forth. A summary of the labeling scheme is given in Table 3. The oxygen atoms are labeled sequentially.

Table 2. Atomic Positions of $Na_{0.40(2)}MnO_2$ at 5 K As Determined from Rietveld Analysis of Synchrotron X-ray Data[a]

atom	*x*	*y*	*z*	occupancy
Mn11	0.0 (−)	0.5 (−)	0.0 (−)	1 (−)
Mn12	0.0 (−)	0.5 (−)	0.5 (−)	1 (−)
Mn13	0.0 (−)	0.5 (−)	0.2515 (2)	1 (−)
Mn21	0.3601 (10)	0.3091 (3)	0.1275 (2)	1 (−)
Mn22	0.3686 (10)	0.3068 (3)	0.6247 (2)	1 (−)
Mn31	0.0225 (9)	0.1114 (3)	0.2495 (1)	1 (−)
Mn32	0.0137 (2)	0.1111 (5)	0.0 (−)	1 (−)
Mn33	0.0088 (2)	0.1098 (5)	0.5 (−)	1 (−)
Mn41	0.0325 (10)	0.3085 (2)	0.2502 (1)	1 (−)
Mn42	0.0304 (2)	0.3034 (5)	0.0 (−)	1 (−)
Mn43	0.0365 (2)	0.3021 (4)	0.5 (−)	1 (−)
Mn51	0.3605 (8)	0.0916 (2)	0.1251 (1)	1 (−)
Mn52	0.3500 (8)	0.0853 (2)	0.6236 (1)	1 (−)
O1	0.3647 (3)	0.0060 (7)	0.1319 (4)	1 (−)
O2	0.3528 (3)	−0.0027 (8)	0.6181 (3)	1 (−)
O3	0.0497 (3)	0.1623 (10)	0.1112 (3)	1 (−)
O4	0.0595 (3)	0.1608 (11)	0.6224 (4)	1 (−)
O5	0.4262 (3)	0.1684 (8)	0.1280 (4)	1 (−)
O6	0.4106 (3)	0.1594 (8)	0.6175 (4)	1 (−)
O7	0.1701 (3)	0.2863 (9)	0.1130 (3)	1 (−)
O8	0.1603 (3)	0.2810 (9)	0.6067 (3)	1 (−)
O9	0.4625 (3)	0.4319 (8)	0.1195 (4)	1 (−)
O10	0.4769 (3)	0.4375 (8)	0.6322 (4)	1 (−)
O11	0.2131 (3)	0.1010 (7)	0.2475 (3)	1 (−)
O12	0.4118 (3)	0.2628 (10)	0.2355 (3)	1 (−)
O13	0.3430 (3)	0.3558 (9)	0.2492 (4)	1 (−)
O14	0.4951 (4)	0.0757 (10)	0.2517 (4)	1 (−)
O15	0.2146 (5)	0.0826 (4)	0.0 (−)	1 (−)
O16	0.4370 (4)	0.2757 (3)	0.0 (−)	1 (−)
O17	0.2993 (5)	0.3656 (1)	0.0 (−)	1 (−)
O18	0.5095 (5)	0.0618 (1)	0.0 (−)	1 (−)
O19	0.2279 (6)	0.0887 (2)	0.5 (−)	1 (−)
O20	0.4119 (5)	0.02628 (2)	0.5 (−)	1 (−)
O21	0.3136 (5)	0.3534 (2)	0.5 (−)	1 (−)
O22	0.4864 (6)	0.0763 (2)	0.5 (−)	1 (−)
Na11	0.2270 (5)	0.1895 (2)	0.0 (−)	0.34 (2)
Na12	0.2277 (3)	0.2093 (9)	0.2241 (2)	0.75 (3)
Na13	0.2038 (3)	0.2142 (1)	0.5 (−)	0.54 (2)
Na21	0.2491 (3)	0.4418 (9)	0.2231 (2)	0.60 (2)
Na22	0.1947 (1)	0.4146 (5)	0.6301 (3)	1.0 (2)
Na31	0.1131 (5)	0.0195 (1)	0.5 (−)	0.35 (2)
Na32	0.1292 (4)	0.0001 (2)	0.2545 (5)	0.50 (3)
Na33	0.1138 (6)	0.0022 (3)	0.0 (−)	0.28 (2)

[a] Lattice parameters were a = 9.06361(4) Å, b = 26.4024(1) Å, and c = 11.28497(3) Å. *R*-factor = 6.54. Space group, *Pnnm*.

Table 3. Summary of Mn Site Labels in the High and Low Temperature Configurations, along with Average Mn−O Bond Distances

high temperature (*a b c*) cell		low temperature (*a b* 4*c*) cell	
atom label	average bond Mn−O distance (Å)	atom label	average bond Mn−O distance (Å)
Mn1 (4+)	1.9101	Mn11	1.9248
		Mn12	1.8187
		Mn13	1.9510
Mn2 (4+)	1.8990	Mn21	1.9023
		Mn22	1.9320
Mn3 (4+)	1.8871	Mn31	1.9141
		Mn32	1.9562
		Mn33	1.9311
Mn4 (3+)	1.9465	Mn41	2.0361
		Mn42	1.9489
		Mn43	1.9035
Mn5 (3+)	2.0216	Mn51	2.0418
		Mn52	1.9917

Sodium Position and Occupancy. In the high temperature structure, there were three Na chains: Na1 in the smaller channel and two in the "S" shaped channel, labeled Na2 and Na3. A projection of these three chains in the low temperature structure is given in Figure 5. The Na1 and Na3 share a number of common features at low temperature. First, Na1 and Na3 chains both generate three new Na positions labeled Na11, Na12, and Na13 and Na31, Na32 and Na33, respectively. Two of the positions for each chain, Na11, Na13 and Na31, Na33, occupy special positions along the *c* direction, and they only have degrees of freedom in the *xy* plane and in their occupancy. The third positions at (x y ∼0.25) are free to refine to any location and occupancy, but in fact both chains remain very close to the high temperature structure. For example, Na32 adopts a position along *c* at z = 0.2545(5), very close to the ideal, z = 0.25. A more significant departure from the high temperature structure is the modulation or curvature the Na1 and Na3 chains adopt at low temperature. The distortion is still subtle for both Na1 and Na3 chains, but interestingly almost identical. For example, Na1 is located at y = 0.2065(6) at 500 K; at low temperature the y coordinate ranges from Na11 (0.1895(2)), Na12 (0.2093(9)) and Na13 (0.2142(1)) on traveling up the *c*-axis. In other words, whereas the average position is roughly equal, the position modulates down the *c*-axis and deviates from the high temperature structure that has a fixed y coordinate. The fact that these two chains are so similar may be a result of another commonality; they are both located in the central of the channels and are thereby experiencing similar interactions with the framework. For Na1, the occupancy of the low temperature sites, Na11, Na12, and Na13, averages to a value similar to that observed at high temperature. This is expected, as the extent of diffusion between the channels is likely to be low, and the Na are mostly confined to within the small channel. In contrast, the ratio of the two sites within the "S" shaped channel at high temperature is Na2:Na3 of 0.39(3):0.61(3). This ratio is reversed at low temperature, such that the middle sites (Na31, Na32, and Na33) have occupancies of between 0.28(2) and 0.5(3), whereas the Na21 and Na22 positions range from 0.60(2) to 1.00(2) occupancy. The second Na chain in the "S" shaped channel that generates Na21 and Na22 at low temperature follows the same general trend to form a curved modulation with highest occupancy at central positions. However, the distortion is much more extreme; Na22 takes up two central positions down *c* at z = 0.6301(3) and 0.3699 (3) that are very close to ideal positions of z = 0.625 and 0.375 from the high temperature cell. Na21, in contrast, shifts to z = 0.2231(2) along the *c* axis, which is far from the z = 0.125 ideal position and is actual

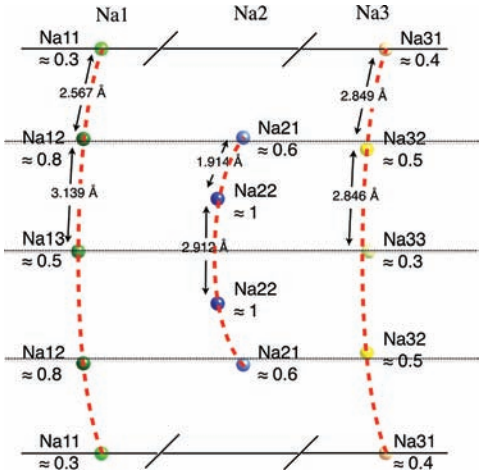

Figure 5. Projection of the Na positions in the *yz* plane, showing the Na1 and Na3 channels in the high temperature cell (see Figure 1) split into Na11, Na12, Na13 and Na31, Na32, Na33, respectively. They are positioned down the *c*-axis close to their ideal high temperature locations, indicated by the dotted line, but adopt a curved or modulated arrangement with respect to the *xy* plane. In contrast, Na2 channel (Figure 1) splits into Na21 and Na22, where the latter adopts positions similar to the ideal structure, whereas Na21 shifts greatly toward the center for the cell as well as in the *xy* plane, forming a highly curved arrangement.

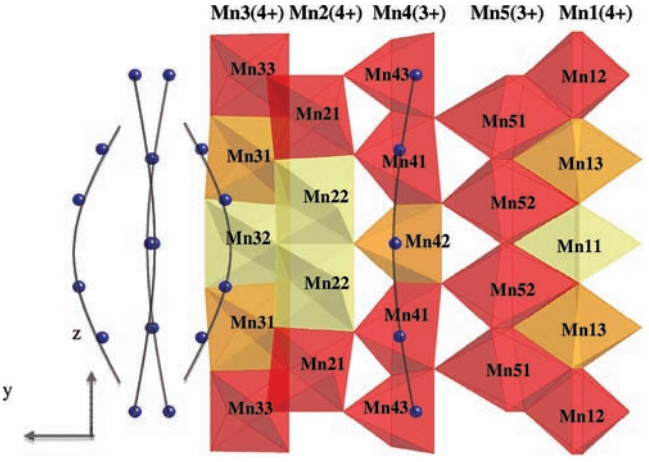

Figure 6. Structure of $Na_{0.40(2)}MnO_2$ at 5 K, as determined from Rietveld refinement of synchrotron X-ray data, showing the (*a b* 4*c*) cell results from a modulation in both the Na positions and the distortion to the MnO_6 and MnO_5 units, caused by variable charge distribution. The labels above the polyhedra indicate the Mn position in the high temperature structure used to label Figure 1.

closer to the unit cell edge in the original cell at $z = 0.25$. Moreover, the x coordinate for Na21 is $x = 0.2491(3)$ as compared to $x = 0.1947(1)$ for Na22, forming a much more convex profile than the two central chains. The other two chains in the "S" shaped channel, providing four in total, are generated by the 2-fold rotation axis and are therefore in phase with each other. It is important to note that the equivalent Na positions in an adjacent "S" shaped channel are shifted by $z = 0.5$ with respect to each other, as a result of the glide plane, *n*, symmetry term.

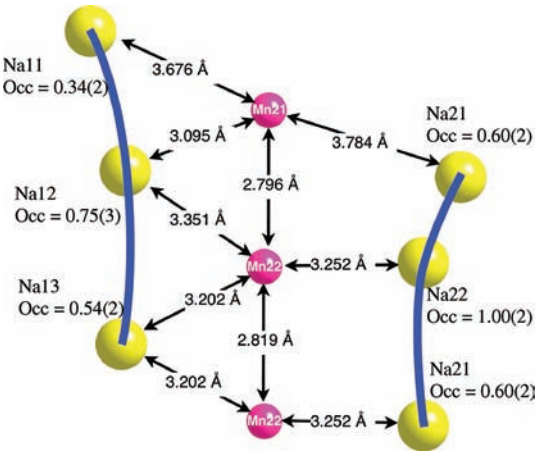

Figure 7. A typical section of the $Na_{0.40(2)}MnO_2$ structure. Mn22, which shows an MnO_6 environment consistent with much Mn^{4+} character, is associated with shorter Mn−Na bond distance as compared to the highly distorted ion, Mn21, with greater Mn^{3+} character.

Manganese Charge and Orbital Ordering. Figure 6 shows the inequivalent Na and Mn−O polyhedra that form the structure of $Na_{0.40(2)}MnO_2$ in the *yz* plane. One important question that arises is whether the superlattice reflections are simply a result of the Na ordering or in addition the structure is associated with modulation of the Mn charge and orbital ordering. In an attempt to clarify this, the bond variance was calculated to estimate the extent of the distortion to each of the 13 Mn−O environments. A summary of this calculation is given in the Supporting Information. The calculation showed that, although the general trend was unaffected, the Mn that make up the Mn^{3+} chains (Mn41, Mn42, Mn43, Mn51, and Mn52) remained highly distorted on average at low temperature. Similarly, those Mn sites that were 4+ at high temperature (Mn11, Mn12, Mn13, Mn21, Mn22, Mn31, Mn32, and Mn33) were still, on average, more consistent with a Mn^{4+} description at low temperature. There were significant perturbations to the charge modulations along the quadrupled *c*-axis, such that the Mn ions that were symmetrically equivalent at higher temperatures adopt different configurations as a result of the Na ordering. The octahedral Mn^{3+} chains (Mn5 at high temperature), which are made up of Mn51 and Mn52 ions at low temperature, are highly distorted throughout the entire chain, whereas the square pyramid chain, labeled as Mn4 in the high temperature structure that results in Mn41, Mn42, and Mn43 in the low temperature configuration, possesses bond variance of 0.069, 0.100, and 0.196, respectively. This suggests that there is a variation of the extent of the Mn distortion as a function of its location down the *c*-axis, such that positions closer to the supercell edges are more distorted than those in central locations. Mn11, Mn13, and Mn12 (high temperature Mn1 in Figure 1) have bond variance of 0.053, 0.083, and 0.12, respectively, thereby showing a similar tendency for the more distorted cations with more Mn^{3+} character to adopt positions at the supercell edges. Mn22 and Mn21 (high temperature Mn2 in Figure 1) have bond variance of 0.051 and 0.097, whereas Mn32, Mn31, and Mn33 (high temperature Mn3 in Figure 1) have bond variance of 0.055, 0.081, and 0.102, respectively. To summarize this diagrammatically, the Mn−O units, shown in Figure 6, are broken into three catagories; red represents highly distorted and therefore most Mn^{3+} in character, and the lighter colors represent a

reduction in the Jahn−Teller distortion and therefore inclusion of more Mn^{4+} character, assignment of which is based on the value of their bond variance. This directly correlates with the occupancy of the Na positions discussed earlier, such that the Mn^{3+} is associated with a depopulation of the Na sites, whereas Mn^{4+} lies in regions of the structure with high Na occupancy. It demonstrates that the Coulombic interaction between the modulated Na positions and Mn−O chains directly affects the Mn charge and orbital ordering.

The coupling between the Na positions and occupancies with the Mn charge and orbital ordering is represented in more detail in Figure 7. Mn22 ions, which show more Mn^{4+} character and are located halfway along the *c* unit cell, are close to fully populated Na22 ions, Na13 (occupancy ∼0.5) and Na12 (occupancy of 0.7), at relatively short Na−Mn distances. In contrast, Mn21 ions that are highly distorted and possess more Mn^{3+} character are positioned near the unit cell edges and are close to Na ions with the low occupancy (Na11, occupancy 0.3) at much longer distances than those observed for Mn22. The close relationship between the Mn charge and Na position and occupancy would greatly benefit from accurate computational calculations. A detailed analysis of the Na−Mn bond distances is provided in the Supporting Information.

CONCLUSIONS

Charge ordering occurs in $Na_{0.40(2)}MnO_2$ such that there are three crystallographically distinct Mn^{4+} octahedral sites, and an octahedra and a square pyramidal Mn^{3+} site, which remain to temperatures above 700 K before the structure collapses on Na loss. The formula, as such, is best written as $Na_{0.4}{}^{+}Mn_{0.4}{}^{3+}Mn_{0.6}{}^{4+}O_2$. The presence of the Mn^{3+} Jahn−Teller active ion can be observed in detail from bond length variance. However, inspection of the average bond length at 500 K (see Table 3) shows the Mn^{4+} ions (Mn1, Mn2, and Mn3) have values of 1.9101 Å or below, whereas the larger Mn^{3+} ion has an average bond length of 1.9465 Å or above. Below a sodium ordering transition at $T_{Na} \approx$ 310 K, direct coupling between the charge of the Mn sites and location of the ordered Na positions occurs to produce a commensurate structure with a (0 0 1/4) propagation vector. A modulation down the quadrupled *c*-axis of both the Na positions and the occupancy resides in parallel with an associated modulation of the extent of the Mn−O distortion, and therefore the Mn charge, such that the greatest distortion and thereby most Mn^{3+} character occurs at furthest Mn−Na distance and lowest Na occupancy, whereas short Mn−Na distances and highest Na occupancies occur for Mn ions with the most Mn^{4+} character. Previous structures in the Na−Mn−O phase diagram have displayed an opposite relationship. Structures with the presence of Mn^{4+} ions, such as $NaMn_7O_{12}$,[25] have longer Na−Mn distance as compared to those possessing only Na−Mn^{3+} bond distance, such as α-$NaMnO_2$ itself.[8]

ASSOCIATED CONTENT

Supporting Information. Additional details on the anisotropic broadening, bond variance calculations, and symmetry analysis. This material is available free of charge via the Internet at http://pubs.acs.org.

AUTHOR INFORMATION

Corresponding Author
mark.green@nist.gov

REFERENCES

(1) Khomskii, D. I.; Sawatzky, G. A. *Solid State Commun.* **1997**, *102*, 87.
(2) Rao, C. N. R.; Arulraj, A.; Cheetham, A. K.; Raveau, B. *J. Phys.: Condens. Matter* **2000**, *12*, R83.
(3) Rao, C. N. R.; Cheetham, A. K. *Adv. Mater.* **1997**, *9*, 1009.
(4) Goodenough, J. B. *Phys. Rev.* **1955**, *100*, 564.
(5) Rodriguez-Carvajal, J.; Hennion, M.; Moussa, F.; Moudden, A. H. *Phys. Rev. B* **1998**, *57*, R3189.
(6) Kimura, T.; Kawamoto, S.; Yamada, I.; Azuma, M.; Takano, M.; Tokura, Y. *Phys. Rev. B* **2003**, *67*, 180401.
(7) Atou, T.; Chiba, H.; Ohoyama, K.; Yamaguchi, Y.; Syono, Y. *J. Solid State Chem.* **1999**, *145*, 639.
(8) Giot, M.; Chapon, L. C.; Androulakis, J.; Green, M. A.; Radaelli, P. G.; Lappas, A. *Phys. Rev. Lett.* **2007**, *99*, 247211.
(9) Stock, C.; Chapon, L. C.; Adamopoulos, O.; Lappas, A.; Giot, M.; Taylor, J. W.; Green, M. A.; Brown, C. M.; Radaelli, P. G. *Phys. Rev. Lett.* **2009**, *103*, 077202.
(10) Ji, S.; Kan, E. J.; Whangbo, M.-H.; Kim, J.-H.; Qiu, Y.; Matsuda, M.; Yoshida, H.; Hiroi, Z.; Green, M. A.; Ziman, T.; Lee, S.-H. *Phys. Rev. B* **2010**, *81*, 094421.
(11) Feng, Q.; Kanoh, H.; Ooi, K. *J. Mater. Chem.* **1999**, *9*, 319.
(12) Parant, J. P.; Olazcuag, R.; Devalett, M.; Fouassie, C.; Hagenmul, P. *J. Solid State Chem.* **1971**, *3*, 1.
(13) Doeff, M. M.; Peng, M.; Ma, Y. P.; Dejonghe, L. C. *J. Electrochem. Soc.* **1994**, *141*, L145.
(14) Doeff, M. M.; Richardson, T. J.; Kepley, L. *J. Electrochem. Soc.* **1996**, *143*, 2507.
(15) Armstrong, A. R.; Huang, H.; Jennings, R. A.; Bruce, P. G. *J. Mater. Chem.* **1998**, *8*, 255.
(16) Chu, Q.; Wang, X.; Li, Q.; Liu, X. *Acta Crystallogr.* **2011**, *C67*, i10.
(17) Hadermann, J.; Abakumov, A. M.; Gillie, L. J.; Martin, C.; Hervieu, M. *Chem. Mater.* **2006**, *18*, 5530.
(18) Becker, D. F.; Casper, J. S. *Acta Crystallogr.* **1957**, *10*, 332.
(19) Gillie, L.; Hadermann, J.; Perez, O.; Martin, C.; Hervieu, M.; Suard, E. *J. Solid State Chem.* **2004**, *177*, 3383.
(20) Brock, S.; Duan, N.; Tian, Z.; Giraldo, O.; Zhou, H.; Suib, S. *Chem. Mater.* **1998**, *10*, 2619.
(21) Feng, Q.; Kanoh, H.; Ooi, K. *J. Mater. Chem.* **1999**, *9*, 319.
(22) Rodriguez-Carvajal, J. *Physica B* **1993**, *192*, 55.
(23) Mumme, W. *Acta Crystallogr., Sect. B* **1968**, *24*, 1114.
(24) Aroyo, M. I.; Perez-Mato, J. M.; Capillas, C.; Kroumova, E.; Ivantchev, S.; Madariaga, G.; Kirov, A.; Wondratschek, H. *Z. Kristallogr.* **2006**, *221*, 15.
(25) Prodi, A.; Gilioli, E.; Gauzzi, A.; Licci, F.; Marezio, M.; Bolzoni, F.; Huang, Q.; Santoro, A.; Lynn, J. W. *Nat. Mater.* **2004**, *3*, 48.